Identification of Non-Fermi Liquid Physics in a Quantum Critical Metal via Quantum Loop Topography

George Driskell,[1] Samuel Lederer,[1] Carsten Bauer,[2] Simon Trebst,[2] and Eun-Ah Kim[1,*]
[1]*Department of Physics, Cornell University, Ithaca, New York 14853, USA*
[2]*Institute for Theoretical Physics, University of Cologne, 50937 Cologne, Germany*

(Received 25 November 2020; accepted 23 June 2021; published 22 July 2021)

Non-Fermi liquid physics is ubiquitous in strongly correlated metals, manifesting itself in anomalous transport properties, such as a T-linear resistivity in experiments. However, its theoretical understanding in terms of microscopic models is lacking, despite decades of conceptual work and attempted numerical simulations. Here we demonstrate that a combination of sign-problem-free quantum Monte Carlo sampling and quantum loop topography, a physics-inspired machine-learning approach, can map out the emergence of non-Fermi liquid physics in the vicinity of a quantum critical point (QCP) with little prior knowledge. Using only three parameter points for training the underlying neural network, we are able to robustly identify a stable non-Fermi liquid regime tracing the fans of metallic QCPs at the onset of both spin-density wave and nematic order. In particular, we establish for the first time that a spin-density wave QCP commands a wide fan of non-Fermi liquid region that funnels into the quantum critical point. Our study thereby provides an important proof-of-principle example that new physics can be detected via unbiased machine-learning approaches.

DOI: 10.1103/PhysRevLett.127.046601

Correlated electrons can give rise to a wide range of different macroscopic quantum phenomena, yet there is one recurring quantum many-body state of central importance —the non-Fermi liquid (NFL), which is found in the vicinity of such distinct states as quantum critical metals, superconductors, and fractionalized quantum matter. Conceptually, NFLs are systems of interacting electrons that evade a description in terms of Landau's Fermi liquid theory of metals [1,2]. Experimentally, this is often established via the observation of deviations from Fermi liquid phenomenology, such as the absence of a constant specific heat coefficient or, more typically, in transport measurements that show a deviation from a T^2 dependence of the resistivity at low temperatures [3]. In fact, the almost perfect T-linear resistivity above the superconducting dome [which likely masks a quantum critical point (QCP)] in a number of $3d$ transition metal oxides has been an experimental hallmark of what is widely dubbed a "strange metal" regime [4]. Developing a theoretical understanding of such non-Fermi liquid physics and establishing its microscopic origin(s) has, however, remained one of the major outstanding challenges of condensed matter theory for decades.

Conceptual difficulties in studying NFL physics near QCPs have arisen along multiple fronts: (i) The interaction of gapless modes of the bosonic order parameter with the profusion of Fermi surface excitations has hampered efforts toward a controlled analytical treatment [5–12]. (ii) The numerical analysis of many-electron systems has seen similar roadblocks—either in the form of the sign problem [13] in fermionic quantum Monte Carlo (QMC) approaches or the accelerated growth of entanglement [14,15] in tensor network approaches. (iii) Even in models that permit some exact understanding, the characteristic transport quantities revealing NFL physics are notoriously difficult to calculate. This is because they are nonequilibrium properties and, therefore, require the analytical continuation of imaginary-time correlations to real time in QMC approaches (a numerically ill-posed problem). In addition, Green's functions, which are most straightforward to compute, cannot yield transport information unless vertex corrections happen to vanish [16–18]. The conundrum is that it is the transport experiments that strikingly anchor the NFL regions to the QCPs in most experiments [4].

Recently, however, there has been significant progress in numerical efforts. In a vanguard line of research, a new family [19] of microscopic spin-fermion models has been formulated, each of which is devoid of the infamous sign problem by construction [20,21]. These models have allowed numerically exact studies of quantum criticality in metals undergoing a variety of phase transitions [19, 22–29]. The possibility of NFL physics in the vicinity of such quantum critical behavior has been preliminarily explored in numerical experiments using a variety of imaginary-time proxy observables. While such proxies suggest a breakdown of Fermi liquid behavior, more direct measures of transport phenomena are desired to map out the putative NFL regime in the phase diagrams of these models. As a first step in this direction, it has recently been argued that a combination of QMC sampling and quantum loop topography (QLT)—a physics-inspired machine-learning algorithm—is capable of qualitatively probing transport properties [30]. Proof-of-principle calculations of this QMC + QLT approach, probing the onset of superconductivity in two microscopic models, have yielded striking consistency with numerically exact results for these systems [31].

In this Letter, we demonstrate that this combination of machine-learning assisted analysis and sign-problem-free Monte Carlo sampling (QMC + QLT) can consistently map out a non-Fermi liquid regime in the finite-temperature phase diagram of two representative spin-fermion models involving antiferromagnetic spin-density wave (SDW) order and Ising nematic order, respectively. Both models are found to exhibit a fanlike NFL regime above their respective QCPs, which our QMC + QLT approach identifies without any prior knowledge about NFL physics *per se*, nor its rough location in parameter space. This is accomplished by training the respective neural networks to distinguish the quantum states at only *three* parameter points—one in the ordered phase [32], one in the low-temperature Fermi liquid on the disordered side of the QCP, and one in the high-temperature regime. Our main results for the observation of a broad NFL regime tracing out a fan above the QCP are illustrated in Fig. 1 for the two microscopic models exhibiting SDW and nematic order, respectively. In what follows, we first describe our QLT-based method of data analysis, then present the findings upon applying the method to QMC data for both the SDW and nematic models, and finally discuss the significance of our findings in the contexts of both NFL physics and the broader machine-learning effort in physics research.

Our study builds on work using neural networks to identify quantum [33] and thermal [34] phase transitions in systems of itinerant electrons. Here, we significantly expand on these approaches to map out a non-Fermi liquid regime by employing the QLT preprocessing method [30,35] illustrated in Fig. 2. The neural network takes as input samples of the equal-time Green's function drawn from QMC simulations. Green's function values are multiplied together in triangular and quadrilateral chains involving nearest and next-nearest neighbors to form "loop" variables. The ability of such loop correlations to capture transport properties is explicitly demonstrated for a simple model in the Supplemental Material, Sec. IV [36].

The entire set of these loop variables is then fed into a fully connected feed forward artificial neural network (ANN) with a single hidden layer of ten sigmoid neurons. This network is then trained in order to, as best as possible, output zero for input from within a FL regime and one for NFL. The training is accomplished by labeling data from a small number of points in parameter space (white squares in Fig. 1 labeled 0, black circles labeled 1) and then minimizing by stochastic gradient descent the binary cross entropy between these labels and the output of the network. The trained network is then used to classify the quantum states at arbitrary points across the phase diagram, relying only on the fermionic equal-time Green's functions, a choice that renders our approach universally applicable to any itinerant fermion data.

QCPs in itinerant electron systems fall into one of two classes, depending on how the Fermi surface changes upon entering the ordered phase. In one class, a gap opens up at select points on the Fermi surface due to an ordering with a

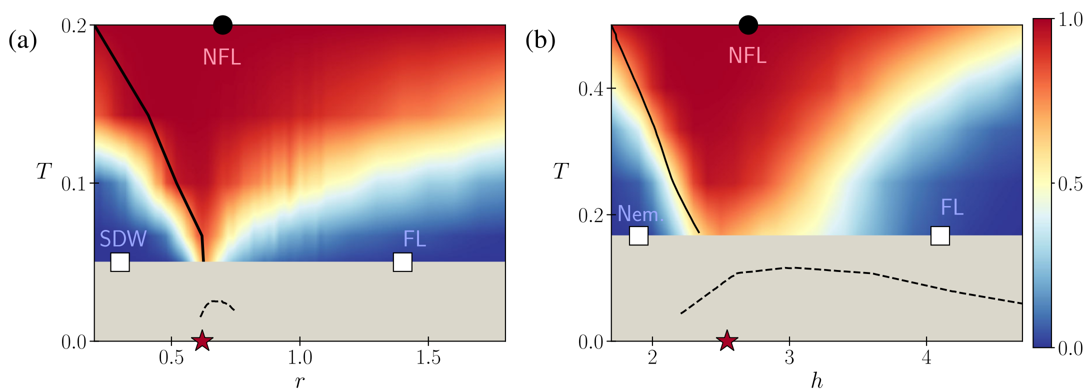

FIG. 1. Machine learning of non-Fermi liquid physics. Phase diagrams of quantum critical metals overlaid with machine-learned Fermi liquid to non-Fermi liquid crossover. The color maps show the output of neural networks trained to classify Fermi liquid (FL) and non-Fermi liquid regimes of the SDW model: [(a) Eq. (1), with $\lambda = 1.5$, $c = 3$, $u = 1$, $\mu = -0.5$] and the nematic (Nem.) model [(b) Eq. (2), with $\alpha = 1.5$, $V = 0.5$, $\mu = -1$]. A value of 1 (dark red) corresponds to the non-Fermi liquid, a value of 0 (dark blue) corresponds to the Fermi liquid, and intermediate values represent the crossover region. The gray regions have been excluded from the present Letter to minimize the confounding effects of superconducting fluctuations. The neural networks are trained on samples of the equal-time Green's function drawn from quantum Monte Carlo simulations, preprocessed using QLT, at the training points shown in the figure: white boxes for the Fermi liquid [(a) $r = 0.3$, $T = 0.05$ and $r = 1.4$, $T = 0.05$; (b) $h = 1.9$, $T = 0.17$ and $h = 4.1$, $T = 0.17$] and black circles for the non-Fermi liquid [(a) $r = 0.7$, $T = 0.2$; (b) $h = 2.7$, $T = 0.5$]. The red stars mark quantum critical value of the tuning parameters [(a) $r_c = 0.62$; (b) $h_c = 2.6$]. The solid black lines show the phase boundaries, and the dashed black lines show the superconducting T_c, from Refs. [23,26].

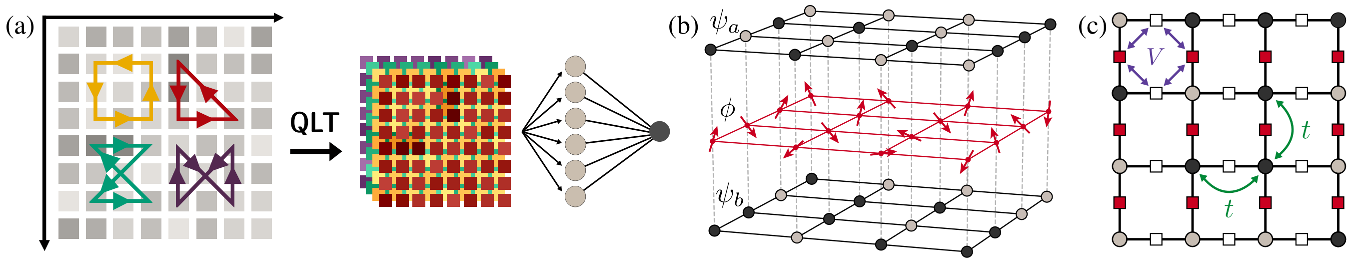

FIG. 2. Architecture of the quantum loop topography approach (a). A dimensional reduction of the full Green's function data is obtained by only considering correlations along (short) spatial loops. For illustration purposes, only four exemplary loops (yellow, red, green, purple) are shown. The resulting quantum loop vector field (colored lattices) are fed into a maximally connected feed forward neural network. Illustration of the lattice models of Eq. (1) featuring (b) a SDW QCP and Eq. (2) hosting (c) an Ising nematic QCP. In the former case (b), two flavors of fermions ψ_x, ψ_y interact with an antiferromagnetic two-component order parameter ϕ described by a ϕ^4 theory. In the latter (c), fermions interact with antiferromagnetically coupled Ising pseudospins (squares) situated on the lattice bonds and subject to a transverse field. Based on Fig. 2 of Ref. [31] and Fig. 3 of Ref. [25], respectively.

finite wave vector $\mathbf{Q}$. Density waves such as spin- and charge-density waves belong to this class. In the other class, no gap opens anywhere, but most of the Fermi surface, if not all, is affected due to a uniform $\mathbf{Q} = 0$ ordering. Nematic order and ferromagnetic order belong to this latter class. We study representative examples from both classes [19,37]. For the first class, we study a sign-problem-free spin-fermion system, see Fig. 2(b), that has been investigated by some of us in extensive, numerically exact determinant quantum Monte Carlo (DQMC) studies [22,23]. The action of the two-dimensional lattice model is given by $S = S_\psi + S_\varphi + S_\lambda$, with

$$S_\psi = \int_{\tau,\mathbf{k}} \sum_{s,\alpha} \psi^\dagger_{\alpha\mathbf{k}s}(\partial_\tau + \epsilon_{\alpha\mathbf{k}s} - \mu)\psi_{\alpha\mathbf{k}s},$$
$$S_\phi = \int_{\tau,\mathbf{r}} \left(\frac{r}{2}\phi^2 + \frac{1}{2c^2}(\partial_\tau\phi)^2 + (\nabla\phi)^2 + \frac{u}{4}\phi^4\right),$$
$$S_\lambda = \lambda \int_{\tau,\mathbf{r}} e^{i\mathbf{Q}\cdot\mathbf{r}_i}\phi_\mathbf{r} \cdot \psi^\dagger_{a\mathbf{r}s}\vec{\sigma}_{ss'}\psi_{b\mathbf{r}s'} + \mathrm{H.c.}, \tag{1}$$

where $\alpha = a,\ b$ is a fermion flavor index and $s = \uparrow, \downarrow$ denotes spin. S_ψ describes the free kinetics of two flavors of spin-1/2 fermions $\psi_{\alpha\mathbf{r}s}$ with energy dispersion $\epsilon_{\alpha\mathbf{k}s}$ situated on a square lattice. The antiferromagnetic order parameter ϕ is of easy-plane character and is governed by an O(2) symmetric ϕ^4 theory. The contribution S_λ is a Yukawa-like spin-density coupling with an ordering wave vector $\mathbf{Q} = (\pi, \pi)$, which connects different scattering hot spots on the Fermi surface. As specific model parameters, we choose $\lambda = 1.5$, $c = 3$, and $u = 1$, which puts the QCP at a critical coupling $r_c = 0.62$ [23], masked by the formation of a superconducting dome, as indicated in the lower panel of Fig. 1(a). We exclude from our Letter the range of temperatures (gray region) comparable to the maximum critical temperature in order to minimize the confounding effects of superconducting fluctuations and also do so for the nematic model in Fig. 1(b).

Turning to the numerical analysis of this model and to contrast our QLT approach with a traditional QMC investigation, it is instructive to briefly discuss the results obtained for this model in such a conventional approach [23]. To locate the SDW phase transition of model (1), a careful finite-size scaling analysis is employed using the known properties of the Berezinskii-Kosterlitz-Thouless type phase transition corresponding to the O(2) symmetric SDW order. A superconducting transition, shown as a dashed line in Fig. 1(a), is established by measuring the superfluid density [38]. The nature of fermionic excitations in the vicinity of this QCP (above the superconducting dome) is examined using the Matsubara self-energy extracted from the imaginary time-displaced Green's function. For model (1), the self-energy at the hot spots is found to be finite and only weakly dependent on Matsubara frequency. This is contrary to the Fermi liquid prediction of a quadratic frequency dependence of the self-energy and indicates a loss of coherence [23]. Consequently, the quasiparticle weight at the hot spots drops significantly near the QCP [23]. While this method for detecting a novel non-Fermi liquid state is theoretically appealing and numerically exact, it is associated with considerable computational cost: the calculation of time-displaced Green's functions. Importantly, this cost is incurred for every parameter point of the phase diagram. For this reason, in spite of the DQMC simulations of Ref. [23] having a scope of $\mathrm{O}(10 \times 10^7)$ CPU hours on modern supercomputers, non-Fermi liquid behavior could only be established at a few discrete points, for example $r = 0.7$, $T = 0.05$. Mapping out an extended quantum critical region has so far been out of reach.

As we show in Fig. 1(a), our shallow, fully connected neural network learns the full two-dimensional phase diagram of the model of Eq. (1) when trained with 3200 input vectors from each of the three representative points. The predictions are consistent among independently trained networks, as shown in the Supplemental Material [36]. With just three points to anchor the phase diagram, it is particularly remarkable that the non-Fermi liquid state (supported by the high-temperature training point) extends to the lowest temperatures. Moreover, the formation of a quantum critical fan recognized by the neural network shows the steep rise of the NFL-FL crossover temperature away from the QCP without explicit prior knowledge. The narrowing of the quantum critical fan zooming into the actual QCP is a highly nontrivial feature learned by the network. Indeed, this work represents the first time a non-Fermi liquid quantum critical fan has been firmly established near any magnetic QCP. Even more remarkable is the robustness of the phase diagram against the choice of specific training point locations (see Supplemental Material, Sec. IIA, Fig. 2 [36]). This remarkable robustness should be contrasted with neural networks trained on snapshots of classical order parameters, which require training points also in the immediate vicinity of the phase boundary [39] or otherwise fail.

To further investigate the neural network's learning of the NFL region and the quantum critical fan, we explore a setup where the ANN learns only about the existence of the SDW phase and the FL state by training with only *two sets* of training data for each case. Even though QLT was originally developed as a probe of transport [30], a binary classification using the SDW and disordered phases robustly captures almost the entire phase boundary of the SDW state, as shown in Fig. 3(a). This level of performance without explicit reference to the order parameter is somewhat surprising. We speculate that the gap opened by the SDW order in the vicinity of only four points on the Fermi surface may nonetheless be robustly detectable in the (local) QLT input. A binary classification targeting the FL and disordered states, shown in Fig. 3(b), indicates that the NFL-FL crossover can also be independently learned, even without referencing the ordered phase. The mapping of this crossover, both here and in Fig. 1, represents a major advance, having not been accomplished in the prior literature.

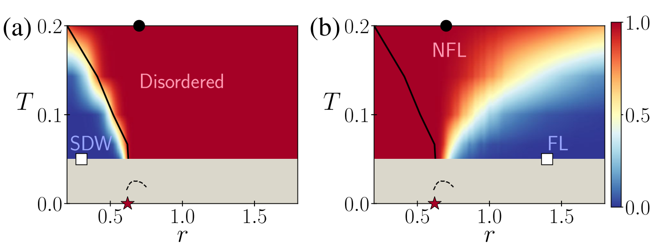

FIG. 3. Binary classification for the SDW model. (a) The neural network is trained to distinguish the quasi-long-range ordered phase (training point at the white box, $r = 0.3$, $T = 0.05$) from the non-Fermi liquid regime (the black circle, $r = 0.7$, $T = 0.2$). (b) The neural network is trained to distinguish the disordered Fermi liquid regime (training point at the white box, $r = 1.1$, $T = 0.05$) from the non-Fermi liquid regime [the black circle, as in (a)].

As a prototype of a QCP to a uniform ($\mathbf{Q} = 0$) order, we consider a sign-problem-free lattice model for Ising nematic quantum criticality [25,26]. As shown in Fig. 2(c), the model's degrees of freedom are fermions $c_{i,\sigma}$ that live on the sites i of a square lattice and pseudospins that live on the nearest-neighbor bonds $\langle i, j\rangle$ coupling to the bond charge density of fermions. The Hamiltonian is $H = H_f + H_b + H_{\mathrm{int}}$, where

$$\begin{aligned} H_f &= -t\sum_{\langle i,j\rangle,\sigma} c^\dagger_{i\sigma}c_{j\sigma} - \mu\sum_{i\sigma} c^\dagger_{i\sigma}c_{i\sigma}, \\ H_b &= V\sum_{\langle\langle i,j\rangle;\langle k,l\rangle\rangle} \tau^z_{i,j}\tau^z_{k,l} - h\sum_{\langle i,j\rangle}\tau^x_{i,j}, \\ H_{\mathrm{int}} &= \alpha t\sum_{\langle i,j\rangle,\sigma}\tau^z_{i,j}c^\dagger_{i\sigma}c_{j\sigma}. \end{aligned} \tag{2}$$

Here, fermion hopping is considered only between nearest-neighbor sites, and the "antiferromagnetic" interaction V between pseudospins on nearest-neighbor bonds drives the nematic order: when the z components of pseudospins on horizontal bonds, i.e., the white squares in Fig. 2(c), differ from those on their neighboring vertical bonds (red squares), the effective hopping of fermions becomes anisotropic because of the spin-fermion coupling [third line of Eq. (2)]. The "transverse field" h frustrates the ordering tendency and introduces dynamics.

The traditional approach of investigating the phase diagram of model (2) starts by determining the phase boundary of the nematic order. Because the nematic order parameter is discrete, any given simulation will be kinetically trapped in one of the two degenerate minima, making QMC snapshots incompatible among different parallel branches. Traditionally this issue is avoided by turning to the order parameter correlation function (i.e., the nematic susceptibility) and its finite-size scaling [40] for the determination of the ordered phase boundary, as it was done in Ref. [26] using the known 2D Ising critical exponents. While rigorous, this technique requires simulations of numerous system sizes and involves some guesswork in determining the phase transition using data collapse.

Here, we take an alternate approach of a "cold start" [41] for h below that of the non-Fermi liquid training point ($h = 2.7$). This kinetic bias proves sufficient to reproduce the known phase boundary using a single system size and without the computation of higher order fermion correlation functions. Since nearest-neighbor Green's functions are conjugate to the order parameter, we provide nearest-neighbor Green's function data to the feature vector in addition to QLT. As shown in Fig. 1, the ANN learns the nematic phase boundary in remarkable agreement with the conventional analysis [26], indicated by the solid line in Fig. 1, down to the lowest temperatures [42].

NFL behavior in the quantum critical region has also been suggested for this model. The self-energy extracted from the single-particle Green's function has an imaginary part that is both large and, as in the SDW model, frequency independent. There is also evidence of non-Fermi liquid transport from various proxies for the DC resistivity, but these are all subject to the considerable ambiguities of all known forms of analytic continuation. Our method identifies a broad NFL fan, similar to the result for the SDW model and consistent with the much more computationally expensive previous methods.

To summarize, we took a data-science approach to the vast volume of data generated by QMC simulations of quantum critical phenomena in models of itinerant fermions coupled to both antiferromagnetic spin-density wave order and Ising nematic order. By simply providing the equal-time single-particle Green's function data, processed using a QLT machine-learning approach that is designed to target transport, we obtained detailed features of the full phase diagrams, including the formation of NFL physics in a quantum critical fan above the QCP, from the raw data for both models. Our analysis relied on the simulations for a single system size and just three training points deep in the relevant phases, but proved remarkably consistent with the traditionally obtained phase boundaries for the ordered phases. However, most notably, the NFL region is clearly and robustly identified directly from the equal-time data.

Our results prove that it is indeed possible to efficiently extract the information relevant for identifying NFL physics encoded in the equal-time, position-space Green's function data directly. Indeed, the full exploration of the quantum critical region from an exact simulation of the SDW model (which in a conventional analysis turned out to be prohibitively expensive) was accomplished for the first time using the QMC + QLT approach described in this Letter. The phase diagram obtained clearly reveals the QCP at $T = 0$, unknown to the ANN, to be the singular anchor of the NFL regime—perhaps the most subtle and mysterious state that itinerant fermions can form. The simplicity and the robustness of our approach, combined with its effectiveness in detecting this subtle state, imply that data-scientific approaches can enable discoveries from the data readily accessible to QMC simulations in future explorations.

S. L. and E.-A. K. acknowledge the support from the U.S. Department of Energy, Office of Basic Energy Sciences, Division of Materials Science and Engineering under Award No. DE-SC0018946. The Cologne group acknowledges partial support from the Deutsche Forschungsgemeinschaft (DFG, German Research Foundation), Projektnummer 277101999, TRR 183 (project B01). The numerical simulations were performed on the JUWELS cluster at FZ Jülich and the CHEOPS cluster at Regional Computing Centre Cologne.

*eun-ah.kim@cornell.edu

[1] F. D. M. Haldane, in Perspectives in Many-Particle Physics, *Proceedings of the International School of Physics "Enrico Fermi," Course CXXI*, edited by R. A. Broglia, J. R. Schrieffer, and P. F. Bortignon (North-Holland, Amsterdam, 1994), pp. 5–29.

[2] N.-P. Ong and R. Bhatt, *More is Different* (Princeton University Press, Princeton, NJ, 2001).

[3] H. Löhneysen, A. Rosch, M. Vojta, and P. Wölfle, Fermi-liquid instabilities at magnetic quantum phase transitions, Rev. Mod. Phys. **79**, 1015 (2007).

[4] S. Sachdev and B. Keimer, Quantum criticality, Phys. Today **64**, 2, 29 (2011).

[5] A. Rosch, Interplay of Disorder and Spin Fluctuations in the Resistivity near a Quantum Critical Point, Phys. Rev. Lett. **82**, 4280 (1999).

[6] L. Dell'Anna and W. Metzner, Electrical Resistivity near Pomeranchuk Instability in Two Dimensions, Phys. Rev. Lett. **98**, 136402 (2007).

[7] D. L. Maslov, V. I. Yudson, and A. V. Chubukov, Resistivity of a Non-Galilean-Invariant Fermi Liquid near Pomeranchuk Quantum Criticality, Phys. Rev. Lett. **106**, 106403 (2011).

[8] S. A. Hartnoll, R. Mahajan, M. Punk, and S. Sachdev, Transport near the Ising-nematic quantum critical point of metals in two dimensions, Phys. Rev. B **89**, 155130 (2014).

[9] A. A. Patel and S. Sachdev, DC resistivity at the onset of spin density wave order in two-dimensional metals, Phys. Rev. B **90**, 165146 (2014).

[10] X. Wang and E. Berg, Scattering mechanisms and electrical transport near an Ising nematic quantum critical point, Phys. Rev. B **99**, 235136 (2019).

[11] V. S. de Carvalho and R. M. Fernandes, Resistivity near a nematic quantum critical point: Impact of acoustic phonons, Phys. Rev. B **100**, 115103 (2019).

[12] L. E. Vieira, V. S. de Carvalho, and H. Freire, DC resistivity near a nematic quantum critical point: Effects of weak disorder and acoustic phonons, Ann. Phys. (Amsterdam) **419**, 168230 (2020).

[13] E. Y. Loh, J. E. Gubernatis, R. T. Scalettar, S. R. White, D. J. Scalapino, and R. L. Sugar, Sign problem in the numerical simulation of many-electron systems, Phys. Rev. B **41**, 9301 (1990).

[14] D. Gioev and I. Klich, Entanglement Entropy of Fermions in Any Dimension and the Widom Conjecture, Phys. Rev. Lett. **96**, 100503 (2006).

[15] M. M. Wolf, Violation of the Entropic Area Law for Fermions, Phys. Rev. Lett. **96**, 010404 (2006).

[16] O. Parcollet and A. Georges, Non-Fermi-liquid regime of a doped Mott insulator, Phys. Rev. B **59**, 5341 (1999).

[17] P. Cha, A. A. Patel, E. Gull, and E.-A. Kim, Slope invariant t-linear resistivity from local self-energy, Phys. Rev. Research **2**, 033434 (2020).

[18] P. Cha, N. Wentzell, O. Parcollet, A. Georges, and E.-A. Kim, Linear resistivity and Sachdev-Ye-Kitaev (SYK) spin liquid behavior in a quantum critical metal with spin-$1/2$ fermions, Proc. Natl. Acad. Sci. U.S.A. **117**, 18341 (2020).

[19] E. Berg, M. A. Metlitski, and S. Sachdev, Sign-problem-free quantum Monte Carlo of the onset of antiferromagnetism in metals, Science **338**, 1606 (2012).

[20] E. Berg, S. Lederer, Y. Schattner, and S. Trebst, Monte Carlo studies of quantum critical metals, Annu. Rev. Condens. Matter Phys. **10**, 63 (2019).
[21] X. Y. Xu, Z. H. Liu, G. Pan, Y. Qi, K. Sun, and Z. Y. Meng, Revealing Fermionic quantum criticality from new Monte Carlo techniques, J. Phys. Condens. Matter **31**, 463001 (2019).
[22] Y. Schattner, M. H. Gerlach, S. Trebst, and E. Berg, Competing Orders in a Nearly Antiferromagnetic Metal, Phys. Rev. Lett. **117**, 097002 (2016).
[23] M. H. Gerlach, Y. Schattner, E. Berg, and S. Trebst, Quantum critical properties of a metallic spin-density-wave transition, Phys. Rev. B **95**, 035124 (2017).
[24] Z. H. Liu, G. Pan, X. Y. Xu, K. Sun, and Z. Y. Meng, Itinerant quantum critical point with fermion pockets and hotspots, Proc. Natl. Acad. Sci. U.S.A. **116**, 16760 (2019).
[25] Y. Schattner, S. Lederer, S. A. Kivelson, and E. Berg, Ising Nematic Quantum Critical Point in a Metal: A Monte Carlo Study, Phys. Rev. X **6**, 031028 (2016).
[26] S. Lederer, Y. Schattner, E. Berg, and S. A. Kivelson, Superconductivity and non-Fermi liquid behavior near a nematic quantum critical point, Proc. Natl. Acad. Sci. U.S.A. **114**, 4905 (2017).
[27] X. Y. Xu, K. Sun, Y. Schattner, E. Berg, and Z. Y. Meng, Non-Fermi Liquid at $(2+1)$D Ferromagnetic Quantum Critical Point, Phys. Rev. X **7**, 031058 (2017).
[28] X. Y. Xu, A. Klein, K. Sun, A. V. Chubukov, and Z. Y. Meng, Identification of non-Fermi liquid fermionic self-energy from quantum Monte Carlo data, npj Quantum Mater. **5**, 65 (2020).
[29] Z. H. Liu, X. Y. Xu, Y. Qi, K. Sun, and Z. Y. Meng, Itinerant quantum critical point with frustration and a non-Fermi liquid, Phys. Rev. B **98**, 045116 (2018).
[30] Y. Zhang, C. Bauer, P. Broecker, S. Trebst, and E.-A. Kim, Probing transport in quantum many-fermion simulations via quantum loop topography, Phys. Rev. B **99**, 161120(R) (2019).
[31] C. Bauer, Y. Schattner, S. Trebst, and E. Berg, Hierarchy of energy scales in an O(3) symmetric antiferromagnetic quantum critical metal: A Monte Carlo study, Phys. Rev. Research **2**, 023008 (2020).
[32] For the SDW model, this is technically the quasi-long-ranged ordered phase.
[33] P. Broecker, J. Carrasquilla, R. G. Melko, and S. Trebst, Machine learning quantum phases of matter beyond the fermion sign problem, Sci. Rep. **7**, 8823 (2017).
[34] K. Ch'ng, J. Carrasquilla, R. G. Melko, and E. Khatami, Machine Learning Phases of Strongly Correlated Fermions, Phys. Rev. X **7**, 031038 (2017).
[35] Y. Zhang and E.-A. Kim, Quantum Loop Topography for Machine Learning, Phys. Rev. Lett. **118**, 216401 (2017).
[36] See Supplemental Material at http://link.aps.org/supplemental/10.1103/PhysRevLett.127.046601 for details on numerical methods, further examination of the robustness of the results, and an argument for the ability of QLT to capture transport properties.
[37] C. Wu and S. C. Zhang, Sufficient condition for absence of the sign problem in the fermionic quantum Monte Carlo algorithm, Phys. Rev. B **71**, 155115 (2005).
[38] D. J. Scalapino, S. R. White, and S. Zhang, Insulator, metal, or superconductor: The criteria, Phys. Rev. B **47**, 7995 (1993).
[39] J. Carrasquilla and R. G. Melko, Machine learning phases of matter, Nat. Phys. **13**, 431 (2017).
[40] K. Binder and D. Heermann, *Monte Carlo Simulation in Statistical Physics: An Introduction* (Springer-Verlag, Berlin Heidelberg, 2010).
[41] The cold start initializes the nematic pseudospins in one of the classical ground states of H_b to bias the Monte Carlo kinetics, thereby ensuring that the simulations converge to the vicinity of a single local minimum.
[42] A neural network trained on nearest-neighbor Green's functions alone also predicts this phase boundary with high accuracy and predicts FL-NFL crossovers similar to those of a network that is also trained with QLT. See Sec. III of the Supplemental Material for details [36].